



A proposed experiment to test gravitational anti-screening and MOND using Sun-Gas giant saddle points

A. Raymond Penner¹

Received: 26 May 2020 / Accepted: 17 September 2020 / Published online: 24 September 2020
© Springer Nature B.V. 2020

Abstract The size and availability of Sun-Jupiter and Sun-Neptune saddle regions are determined. Within these regions the net gravitational field is $\leq 10^{-10} \text{ ms}^{-2}$. These regions are therefore suitable for experiments which can provide evidence for the alternative gravitational theories of MOND and gravitational anti-screening. A particular experiment is outlined where the relative separation between two masses is measured. In the case of the Jupiter hosted saddle region, over the duration of the proposed experiment it is found that the relative separation of the two masses as determined by MOND and gravitational anti-screening is approximately 1.24 cm less than that predicted by Newtonian gravitational theory. In the case of the Neptune hosted saddle region the difference is much greater, being 29.0 cm for the specific example provided. This experiment would therefore be a definitive test of MOND and gravitational anti-screening.

Keywords Gravitational anti-screening · MOND · AQUAL · Dark matter · Saddle point · Saddle point region · Gravity · MOND experiment

1 Introduction

Physics has been standing at a crossroad since Zwicky (1933) first pointed out that galaxies were moving too fast to be bound by their host cluster. Since then, a plethora of rotation curves have shown that stars in the outer regions of galaxies are also moving too fast to be bound by their host galaxy.

There would seem to be two possibilities. Given that GR (for a review: Iorio 2015; Debono and Smoot 2016), along with its non-relativistic approximation Newtonian gravity, has passed all laboratory and solar system tests the idea that some undiscovered particle(s) was responsible for the apparent greater gravitational forces seen with the galaxies and clusters would seem to be the best path to follow. No modification of gravitational theory was needed; hence, the theory of dark matter arose. However, even with the LHC, to date no such dark matter particles have been found.

The other possibility is that current gravitational theory needs to be modified. Just as GR modifies Newtonian theory in strong gravitational fields, it is possible that a modification is needed in very weak gravitational fields such as those found in the outer regions of galaxies and clusters. This possibility gains support from details of galactic rotation curves, for there is found to be a strong correlation between the rotational curves of spiral galaxies and the observed baryonic mass. This is highlighted by the work of McGaugh et al. (2016) who considered 153 spiral galaxies, which extend over a very wide range of physical properties, to determine the relationship between the radial acceleration as determined from the observed rotational curves and the predicted radial acceleration due to the Newtonian gravity from the determined baryonic mass distribution of the galaxies. The following Radial Acceleration Relationship (RAR) was found to provide a very good fit to the data:

$$g = \frac{g_N}{1 - e^{-\sqrt{g_N/g_{o,obs}}}} \quad (1)$$

where g is the true acceleration as determined from the observed rotational curve, g_N is the Newtonian gravitational field as determined from the baryonic mass distribution, and $g_{o,obs}$ is a fitted parameter. For their data set, and their

✉ A.R. Penner
raymond.penner@viu.ca

¹ Department of Physics, Vancouver Island University, 900 Fifth Street, Nanaimo, BC, V9R 5S5, Canada

adopted stellar mass-to-light ratio, the fitted value of this observational parameter was found to be

$$g_{o,obs} = (1.20 \pm 0.02) \times 10^{-10} \text{ ms}^{-2}. \quad (2)$$

In the limit where $g_N \ll g$, (1) simplifies to

$$g = (g_N g_{o,obs})^{1/2}. \quad (3)$$

Substituting $g_N = GM_o/r^2$ and $g = v_c^2/r$ into (3) then leads to

$$v_c^4 = Gg_oM_o, \quad (4)$$

where v_c is the constant rotational speed of stars and gas clouds that is found in the outer regions of a galaxy, i.e. where $g_N \ll g_{o,obs}$, and M_o is the total baryonic mass of the galaxy. The relationship as given by (4) is known as the Baryonic Tully-Fisher Relationship (BTFR). The BTFR is the cornerstone of alternative theories to galactic dark matter.

Of course, any alternative gravitational theory must agree with any experiments or observations that have been carried out within our own solar system. Currently, the limits on any possible deviations from gravitational theory within our solar system are provided by the analysis of the ephemerides of solar system bodies. These observations lead to fairly severe constraints, specifically with regards to the precession rate of Saturn's orbit. Using positional observations of planets and spacecraft, Pitjeva and Pitjeva (2013) have determined that the residual precession rate for Saturn is $-(0.32 \pm 0.47) \text{ mas cy}^{-1}$ and that any unaccounted-for mass, ΔM , within Saturn's orbit ($\sim 10 \text{ AU}$) must be $< 1.7 \times 10^{-10} M_\odot$. Equation (1) leads to a value of $\Delta M \ll 10^{-100} M_\odot$, and therefore is in good agreement with Pitjeva & Pitjeva's value.

This paper will consider two of the alternative theories to dark matter, Modified Newtonian Dynamics or MOND (Milgrom 1983a,b,c; Bekenstein and Milgrom 1984; Famaey and McGaugh 2012; Sanders 2014), and gravitational anti-screening or GRAS (Penner 2016a,b, 2017, 2018). As will be shown, these two theories are fundamentally equivalent and only differ conceptually. Departure from standard Newtonian gravitational theory for these alternative theories only becomes significant when $g_N < 10^{-9} \text{ ms}^{-2}$, which is much less than typical accelerations in the Solar System.

MOND and GRAS are non-linear in nature. This is problematic for that any gravitational field, g_{EXT} , external to the gravitational field that is being considered, needs to be included. This external field effect (EFE) can greatly complicate the analysis. In the outer regions of galaxies, the gravitational field being considered is that due to the particular galaxy while g_{EXT} is the gravitational field at that location

due to the rest of the cosmos. Typically, in these outer regions of galaxies $g_{EXT} \ll g$, and as such g_{EXT} is ignored and the BTFR holds.

In the case where the gravitational field generated by a star within the Galaxy is of concern, the external gravitational field must include that due to the Galaxy itself. Within our region of the Galaxy this gravitational field is $\sim 2 \times 10^{-10} \text{ ms}^{-2}$. Given that the impact of the alternative theories only becomes significant when $g_N < 10^{-9} \text{ ms}^{-2}$, it is seen that the Galactic field cannot be ignored in these cases. With regards to our own Sun, the EFE has a significant impact when using MOND or GRAS to investigate the orbits of comets in the Oort cloud (Penner 2020; Paučo and Klačka 2016; Iorio 2010a) or when considering its effect on interstellar spacecraft (Banik and Kroupa 2019). In proposed testing of MOND using wide binaries (Banik and Zhao 2018), the external Galactic field also needs to be included. Indeed, wide binaries completely rule out versions of MOND without the EFE (Pittordis and Sutherland 2019). In all these cases, the EFE is found to significantly reduce the differences between the results from Newtonian gravitational theory and those from either GRAS or MOND. In the context of MOND, the EFE was also considered as a possible explanation for an apparent anomalous perihelion precession of Saturn (Iorio 2010b). However, with the results of Pitjeva and Pitjeva (2013), this anomaly no longer exists.

It may be surmised that an actual experiment within the inner regions of the solar system to distinguish between Newtonian gravitational theory and the two alternative theories would be near impossible. In this case, even far from any solar system members, the external gravitational field would need to include the field of the Sun itself which, even at a distance of 30 AU, is $g_N = 6.6 \times 10^{-6} \text{ ms}^{-2}$. However, in the vicinity of the planets there will exist a saddle point where the gravitational field generated by the planet will cancel the gravitational field generated by the Sun and the rest of the cosmos. The possibility of using such saddle points as locations in which to test MOND has previously been considered (Bekenstein and Magueijo 2006). Specifically, one could look for anomalous tidal stresses in the vicinity of the saddle points. It had been further proposed to extend the LISA Pathfinder mission and have the spacecraft fly near the Sun-Earth saddle point (Bevis et al. 2010; Magueijo and Mozaffari 2012). The high sensitivity of LISA Pathfinder would have allowed it to detect any anomalous tidal stresses. For certain relativistic versions of MOND it was determined that the spacecraft only needed to fly within several hundred km of the Sun-Earth saddle point to pick up any anomaly. However, with the more common formulations of MOND, namely AQUAL (Bekenstein and Milgrom 1984) and QUMOND (Milgrom 2010) the spacecraft would have needed to pass within a km of the saddle point and even then, a detection of any anomalous tidal stress would be dependent on the specific interpolating function used (Galianni

et al. 2012). Given that the add-on to the mission did not occur, this is in some sense a moot point. It has also been proposed to use Lunar Laser Ranging to search for anomalous time delays for signals which pass within meters of the saddle points hosted by the Moon or by the Earth (Magueijo and Mozaffari 2013). However, again any such anomaly only shows up for certain MOND formulations so that only a positive result would be conclusive.

In this manuscript, an experiment will be proposed that will provide a definitive test of MOND and GRAS, irrespective of the specific formulation. The experiment would take place in a saddle region, where the external gravitational field would be $\leq 1.00 \times 10^{-10} \text{ ms}^{-2}$. This would be a suitable region in which to carry out any experimental test of MOND and GRAS. As will be shown, the size of such a saddle region is fundamentally determined by the mass of the host planet and the strength of the gravitational field at the saddle point due to the rest of the cosmos, which in our case is primarily determined by the Sun. The larger the mass of the host planet and the weaker the gravitational field due to the Sun, the larger the saddle region will be. As such, our focus will be on the outer solar system planets Jupiter and Neptune. The size of the saddle region hosted by these planets will be found to be large enough to carry out the experiment.

2 Alternative gravitational theories

2.1 MOND

MOND is the leading alternative to the theory of dark matter. In one interpretation, MOND involves the modification of the law of inertia. The gravitational field itself is Newtonian but the acceleration of a test particle in this field is as given by (Milgrom 1983a,b,c)

$$\mathbf{g}_N = \mu(a/a_o) \mathbf{a}, \tag{5}$$

where $\mu(a/a_o)$ is an interpolating function such that

$$\mu(a/a_o) \rightarrow 1 \quad \text{for } a \gg a_o \tag{6a}$$

and

$$\mu(a/a_o) \rightarrow \frac{a}{a_o} \quad \text{for } a \ll a_o \tag{6b}$$

where a_o is a parameter to be determined by observations. Condition (6a) is required in order to have consistency with Newtonian theory and condition (6b) is required in order to get agreement with the BTFR for $a_o = g_{o,obs}$.

In another interpretation of MOND, it is the gravitational field that is modified. In Newtonian gravitational theory the

gravitational field is given by $\mathbf{g}_N = -\nabla \Phi_N$, with the potential Φ_N determined by Poisson's equation

$$\nabla \cdot \nabla \Phi_N = 4\pi G \rho_b \tag{7}$$

where ρ_b is the baryonic mass density. In the AQUAL formulation of MOND (Bekenstein and Milgrom 1984) the potential is determined by the following modified Poisson equation

$$\nabla \cdot (\mu(g/g_o) \nabla \Phi) = 4\pi G \rho_b, \tag{8}$$

with the gravitational field given by $\mathbf{g} = -\nabla \Phi$. In spherical symmetry, a relation between \mathbf{g} and \mathbf{g}_N can be found by substituting (7) into (8) which leads to

$$\mathbf{g}_N = \mu(g/g_o) \mathbf{g}. \tag{9}$$

Then, as with (6a)–(6b), the conditions

$$\mu(g/g_o) \rightarrow 1 \quad \text{for } g \gg g_o \tag{10a}$$

and

$$\mu(g/g_o) \rightarrow \frac{g}{g_o} \quad \text{for } g \ll g_o \tag{10b}$$

are required in order to agree with Newtonian gravitational theory and the BTFR.

Equation (8) can also be expressed as;

$$\nabla \cdot \nabla \Phi = 4\pi G(\rho_b + \rho_{PDM}) \tag{11}$$

with

$$\rho_{PDM} = \frac{1}{4\pi G} \nabla \cdot (1 - \mu(g/g_o)) \mathbf{g}. \tag{12}$$

In this form ρ_{PDM} is referred to as phantom dark matter. To be clear though, currently with MOND the only source of the gravitational field is the baryonic mass and phantom dark matter is just an aid in computation.

Many functions will of course fit the conditions (10a)–(10b). Two commonly used functions are the standard interpolating function and the simple interpolating function. The standard interpolating function is given by

$$\mu(g/g_o) = \left(1 + \left(\frac{g_o}{g} \right)^2 \right)^{-1/2} \tag{13}$$

while the simple interpolating function is given by

$$\mu(g/g_o) = \left(1 + \frac{g_o}{g} \right)^{-1}. \tag{14}$$

The relationship between \mathbf{g} and \mathbf{g}_N in the two cases are therefore, by (9), given by

$$g_N = g \left(1 + \left(\frac{g_o}{g} \right)^2 \right)^{-1/2} \tag{15}$$

and

$$g_N = g \left(1 + \frac{g_o}{g} \right)^{-1} \tag{16}$$

respectively. For $g \ll g_o$, both (15) and (16) simplify to

$$g = (g_N g_o)^{1/2} \tag{17}$$

which as before leads to the BTFR. To have agreement with the BTFR it follows that for both interpolating functions $g_o = g_{o,obs}$. For a value of $g_N = 5.93 \times 10^{-5} \text{ ms}^{-2}$, corresponding to the value at 10 AU from the Sun, (13) leads to a value of $\Delta M = 2.0 \times 10^{-12} M_\odot$, well within Pitjeva & Pitjeva’s value. However, the simple interpolating function, (14), leads to a value of $\Delta M = 2.0 \times 10^{-6} M_\odot$, which is well outside of Pitjeva & Pitjeva’s value.

2.2 GRAS

The theory of gravitational anti-screening asserts that an additional non-standard gravitational contribution arises from a distribution of mass dipoles surrounding a given baryonic mass. Given this distribution, analogous to the classical electromagnetic case for a dielectric, the mass density, ρ_V , due to these mass dipoles will be determined by

$$\rho_V = -\nabla \cdot \mathbf{P}_G, \tag{18}$$

where \mathbf{P}_G is the mass dipole moment density. The resulting gravitational field \mathbf{g}_V , due to the mass dipole distribution, will therefore be given by

$$\mathbf{g}_V = G \int_V \frac{\rho_V}{r^2} \hat{\mathbf{r}} dV. \tag{19}$$

Equations (18) and (19) are the gravitational equivalent of the contribution that electric dipoles in a dielectric make to the electric field in electromagnetics. The net gravitational field surrounding a baryonic mass in GRAS will thus be given by

$$\mathbf{g} = \mathbf{g}_N + \mathbf{g}_V. \tag{20}$$

Expressing the dependence that the mass dipole moment density \mathbf{P}_G has on the total gravitational field \mathbf{g} by

$$\mathbf{P}_G = -\frac{1}{4\pi G} f(g/g_o) \mathbf{g}, \tag{21}$$

with g_o being a parameter determined by observations, then leads in the case of spherical symmetry, by (18), (19) and (21), to

$$g_V = g f(g/g_o). \tag{22}$$

The required conditions for the function $f(g/g_o)$ are

$$f(g/g_o) \rightarrow 0 \quad \text{for } g \gg g_o \tag{23a}$$

and

$$f(g/g_o) \rightarrow 1 - \frac{g}{g_o} \quad \text{for } g \ll g_o. \tag{23b}$$

Condition (23a) is required in order to have consistency with Newtonian gravitational theory while condition (23b) is required in order to get agreement with the BTFR.

Many functions will fit the conditions (23a)–(23b). This manuscript will consider the following two functions which have been used previously (Penner 2018, 2020);

$$f(g/g_o) = \left(1 + \frac{g}{2g_o} \right)^{-2} \tag{24}$$

and

$$f(g/g_o) = e^{-g/g_o} \tag{25}$$

In the case of spherical symmetry, the relationship between g and g_N for the two cases can be expressed, using (20) and (22), by

$$g = g_N + g \left(1 + \frac{g}{2g_o} \right)^{-2} \tag{26}$$

and

$$g = g_N + g e^{-g/g_o} \tag{27}$$

respectively. For $g \ll g_o$, both functions reduce to (17) and hence to the BTFR. At 10 AU from the Sun, the values of ΔM are $2.9 \times 10^{-11} M_\odot$ and $\ll 10^{-100} M_\odot$ respectively for (26) and (27). Both of these values are well within Pitjeva & Pitjeva’s result.

In GRAS, Poisson’s equation becomes

$$\nabla \cdot \nabla \Phi = 4\pi G(\rho_b + \rho_V) \tag{28}$$

with, by (18) and (21),

$$\rho_V = \frac{1}{4\pi G} \nabla \cdot f(g/g_o) \mathbf{g}. \tag{29}$$

As can be seen by comparing (11)–(12) and (28)–(29), GRAS is equivalent to the AQUAL formulation of MOND in that the interpolating function $\mu(g/g_o)$ used in AQUAL is equivalent to $1 - f(g/g_o)$. The differences are primarily conceptual. In MOND, it is taken that the only source of the gravitational field is baryonic mass and the resulting field is non-Newtonian. In GRAS the resulting field is Newtonian but the source of the gravitational field must now include the mass contribution due to the divergence of the mass dipole distribution. The phantom dark matter distribution in MOND is equivalent to an actual mass density distribution caused by the mass dipoles in GRAS.

Figure 1 shows a plot of g/g_N versus g_N using (13) and (14) for the two interpolating function from AQUAL and

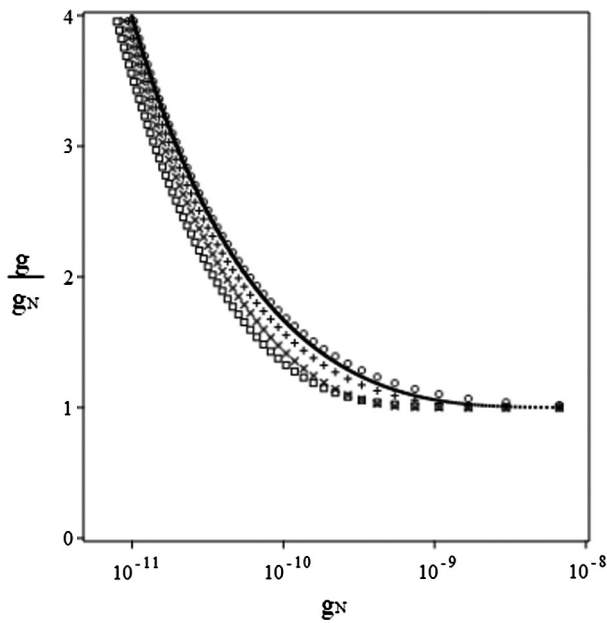


Fig. 1 The dependence that g/g_N has on g_N for: $\circ\circ\circ$ MOND interpolating function (14), $\square\square\square$ MOND interpolating function (13), $+++$ GRAS function (24), $\times\times\times$ GRAS function (25). g_N is in units of ms^{-2} . The solid line is the observed RAR (1)

(24) and (25) for the two functions from GRAS. Of course, as $\mu(g/g_o) = 1 - f(g/g_o)$, these functions are not truly specific to AQUAL or GRAS. In the strong field limit, where $g_N \gg g_o$, all these functions lead to convergence with Newtonian gravitational theory, as expected. In the weak field limit, where $g_N \ll g_o$, all these functions lead to the BTFR, as expected. The functions differ with respect to the RAR which is included in the figure. Although (14) provides the best fit out of the four functions to the RAR, especially for $g_N < 10^{-10} \text{ ms}^{-2}$, this function does not agree with the results of Pitjeva & Pitjeva. The function (24) also provides a good fit to the RAR. As it also agrees with the results of Pitjeva & Pitjeva, it will be the function that is used in the experiment section of the manuscript, i.e. Sect. 4.

Also, as is seen in Fig. 1, MOND and GRAS start to significantly diverge from the Newtonian theory when $g_N < 10^{-9} \text{ ms}^{-2}$. As such, any experimental test of the alternative theories needs to involve the measurement of the gravitational field of a body at a position where its Newtonian gravitational field is $< 10^{-9} \text{ ms}^{-2}$. The difficulty, as discussed in Sect. 1, is the existence of g_{EXT} , the net gravitational field due to the rest of the cosmos. In order to minimize the effect of the external gravitational field, it will also be necessary for any experiment to take place in a region where g_{EXT} is also $< 10^{-9} \text{ ms}^{-2}$.

GRAS should be looked upon as an explanation to the MOND phenomenology given the fundamental equivalence of GRAS and MOND, or at least the AQUAL formulation of MOND. A major aspect of GRAS is that it relies on

the existence of mass dipoles which do not exist in current theory. The following discussion of mass dipoles is as presented in Penner (2020). There have been various models of mass dipoles presented over the years and theories using such mass dipoles to explain astronomical observations currently attributed to dark matter. In general, the cosmos is taken to be filled with mass dipoles, either real or virtual, which by some mechanism align with the gravitational field. In these models of mass dipoles, one of the two particles has its inertial mass, passive gravitational mass, and active gravitational mass all positive. The differences between the models are with respect to the second particle. The simplest case is where the second particle has a positive inertial mass but negative active and passive gravitational masses (Blanchet 2007a; Hajdukovic 2011a,b,c, 2012a,b). Such a mass dipole will align in a gravitational field analogous to an electric dipole in an electric field. Unfortunately, a particle that has its inertial and passive gravitational masses of opposite signs violates the equivalence principle. A model which avoids this is one where the second particle's inertial and passive gravitational masses are positive but whose active gravitational mass is negative (Blanchet 2007b; Blanchet and LeTiec 2008). Although, such a dipole does not violate the equivalence principle, having a particle or dipole whose active gravitational mass is not equal to its passive gravitational mass does violate the law of action and reaction. Additionally, such a dipole will not naturally align in a gravitational field.

A dipole model presented by Bondi (1957) overcomes both problems by having all of the masses, including the inertial mass, of the second particle negative. Such a dipole will have a very strange behavior, in that if the two particles are bound non-gravitationally the dipole will on its own accelerate along the axis joining the two particles in the direction of the negative mass. The dipole moment is therefore anti-parallel to the particle's velocity vector. Indeed, even though it is strange, Bondi has shown that this behavior is allowed in GR as long as the magnitude of the positive mass exceeds that of the negative mass, if only slightly, and if such dipoles come in pairs of opposite orientation. These conditions allow one to define a centre of mass reference frame for the system. Although, such mass dipoles will obey the equivalence principle and will free fall in a gravitational field like any particle, by having each of the component particles with their passive gravitational mass and inertial masses equal, the mass dipoles will again not naturally align in a gravitational field.

In GRAS the mass dipoles are taken to be like Bondi's dipoles, and as such will obey the equivalence principle. However, in GRAS, although it is not strictly necessary, it is proposed that the positive mass component has the same magnitude as the negative mass component. Therefore, overall, the dipole has a net inertial mass, as well as a net active and passive gravitational mass, of zero. Such a massless

dipole will not have a defined centre of mass frame, i.e. like a photon, and there is no reference frame for which the dipole will be at rest.

Also, unlike other theories based on mass dipoles, in GRAS it is not taken that the cosmos is filled with such mass dipoles which then align in a gravitational field. In GRAS the source of the mass dipoles, albeit indirectly, is the baryonic mass itself. A given mass, via its gravitational interactions with other masses, is surrounded by a field of virtual gravitons. These virtual gravitons in turn are taken to have a probability of dissociating into virtual mass dipoles. This picture of virtual mass dipoles is analogous to QED where virtual photons, surrounding a given charge, have a probability of dissociating into virtual electric dipoles. In QED, these temporal virtual electric dipoles come into existence with their electric dipole moment anti-parallel with the electric field. The result in this case is that the virtual electric dipoles cause a screening of the electric charge which greatly reduces the value of the observed charge. In the case of gravitational anti-screening, the virtual mass dipoles come into existence with their mass dipole moment parallel to the gravitational field. The result is an anti-screening effect which greatly increases the value of the observed mass. In GRAS, the answer to the question of what the mass of a given star or galaxy is, is similar to the answer to what is the charge of an electron in QED. Is it the bare charge or the observed charge? Is it the baryonic mass or the observed mass? In the case of the mass of, for example, the Sun the answer is even more complicated as the observed mass is not constant. Within the inner solar system, the effect of the mass dipoles is negligible and to an excellent approximation the mass of the Sun is equal to its baryonic mass, but at distances greater than approximately 5 kAU the observed mass of the Sun rises rapidly. The same of course applies to galaxies which leads to the RAR and the BTFR.

The relationship between the mass dipole moment density and the gravitational field as given by (21), along with the behavior of the function $f(g/g_o)$ as given by (23a)–(23b), is a key step in the theory. The primary justification for this step is that the same relationship between the electric field and the density of the virtual electric dipole moments as given by (21) with functions behaving as (23a)–(23b) leads to a semi-classical model which matches the behavior found in QED, namely that the observed value of a charge falls rapidly from its bare value to a constant observed value (Penner 2016a). Although basing GRAS on a semi-classical model of QED may seem somewhat speculative, it is the author's opinion that a quantum theory of gravity will have similar features to other quantum field theories, including virtual dipoles. The screening of electric charge in QED and the anti-screening of mass in GRAS would then basically be two sides of the same coin.

Another difference between GRAS and other theories which have mass dipoles aligning with the gravitational field

in the manner of electric dipoles in classical electrodynamics is that the other theories lead naturally to the mass dipole moment density saturating in strong fields. This in turn leads to an anomalous constant gravitational field in the inner solar system (Hajdukovic 2013). However, the predictions that follow, i.e. perihelion precession rates, are not in agreement with current observations (Iorio 2019; Banik and Kroupa 2020). In GRAS the mass dipole moment density goes to zero in a strong gravitational field and predictions within the solar system that arise in GRAS (Penner 2020) do not run counter to current observations.

In addition, having the phantom dark matter of MOND being an actual mass density, as it is in GRAS, means that it is no longer required to have an alternative relativistic theory to provide a basis for MOND. In general, alternative relativistic gravitational theories have been found to be problematic (Debono and Smoot 2016), though a relativistic version of MOND has recently been developed in which gravitational waves travel at the speed of light (Skordic and Zlosnik 2019). If one considers the source of the additional gravitational field to be the mass density as given by (18), and not due specifically to individual mass dipoles, the energy-momentum tensor in GR would just need to be altered to

$$T^{\mu\nu} = (\rho_b + \rho_v)u^\mu u^\nu \quad (30)$$

with the Newtonian limit as given by (28). The AQUAL formulation of MOND is then just a way of expressing the gravitational field solely in terms of the baryonic mass. This is analogous to the use of the Displacement vector in classical electromagnetism. However, the theory of GRAS is far from complete, and there are still issues with regards to how it fits in with GR. This it is important to assess the cosmological implications of GRAS.

2.3 Method of solution

The relationship between g and g_N as given by (26) and (27) in GRAS, or (15) and (16) in MOND, only apply to problems of spherical symmetry. In general, to determine the gravitational field for an arbitrary baryonic mass distribution in GRAS requires solving Eqs. (28) and (29). The technique is to take as the initial guess for Φ , that due solely to the baryonic mass, i.e. Φ_N . The resulting distribution for ρ_V is then found from (29) and the next guess for Φ is then found using (28). This is repeated until the differences in g from the previous estimate, through the considered region, are less than a set small amount. This can be quite computationally intensive as the region of space considered must extend significantly beyond the baryonic mass distribution so that the contribution due to the dipoles beyond the considered volume can be neglected. To reduce the computational requirements, problems involving GRAS have been limited to only axisymmetric problems. In these cases, I consider a

Table 1 The gravitational parameters and $(x_{JPL}, y_{JPL}, z_{JPL})$ and (x, y, z) positions of the Sun, Jupiter, and Neptune. Included are the (x_o, y_o, z_o) and y_{op} location of the saddle points and the Δw_{sp} and Δd_{sp} sizes of the corresponding saddle regions as well as Δt_{sp} , the maximum time that a passive body could remain in the saddle region. The bracketed numbers represent the uncertainties

	01-01-2020 00:00.0000	Sun	Jupiter	Neptune
GM (km ³ s ⁻²)		132712440041.93938	126686534.911(1.5)	6835099.5(10)
x_{JPL} (AU)		-0.003798619468	0.522348438935	29.239014044311
y_{JPL} (AU)		0.007439926519	-5.193582583066	-6.359750396991
z_{JPL} (AU)		0.000023030118	0.009853537302	-0.0542875652942
x (AU)		0.003035031537	0	
y (AU)		-0.006462585862		0
z (AU)		-0.007782654272	5.219793581262	
x_o (AU)		-0.005292655619		29.927597320367
y_o (AU)		0.000037721700	0	
z_o (AU)		-0.000072988725		0
y_{op} (AU)			0.00009096150	-0.00004605
Δw_{sp}			5.06312037980(90)	29.71431265(16)
Δd_{sp}			uncertainty = ± 135 m	uncertainty = ± 23.2 km
Δt_{sp}			0.00000113050	-0.00000052
			0.15667322787(90)	0.21328467(16)
			uncertainty = ± 135 m	uncertainty = ± 23.2 km
			10.2 km	475 km
			20.3 km	950 km
			1.88 × 10 ⁴ s = 5.22 h	7.53 × 10 ⁵ s = 209 h

spherical region of space centred on the baryonic mass center. This region is divided into rings whose axes of symmetry lie along the axis of symmetry of the problem.

3 Laboratory

3.1 Location

Consider first the simple case of an isolated Sun-planet system consisting of a planet of mass M_p in orbit at a distance R from the Sun. Treating the planet and the Sun as point masses, and taking that the gravitational field is to an excellent approximation Newtonian, the saddle point of the system will be located at a distance y_{op} from the planet along the axis joining the two as given by

$$g_{\odot} = g_p = \frac{GM_p}{y_{op}^2} \tag{31}$$

where g_{\odot} is the magnitude of the solar gravitational field at the saddle point while g_p is the magnitude of the planetary gravitational field there. With no other bodies in the cosmos, for any experiment carried out at this point the gravitational field $\mathbf{g} = \mathbf{g}_{\odot} + \mathbf{g}_p$ will be equal to zero. For example, consider the Sun-Jupiter, and Sun-Neptune systems. The values of the gravitational parameter GM for the Sun, Jupiter, and Neptune as well as their $(x_{JPL}, y_{JPL}, z_{JPL})$ coordinates with respect to the solar system baryonic centre (SSB) as on Jan 01-2020-00.00.0000, as taken from

<https://ssd.jpl.nasa.gov/?horizons>, are shown in Table 1. Transforming this coordinate system to one where the y-axis lies respectively along either the SSB-Jupiter or the SSB-Neptune axis, leads to the (x, y, z) positions that are also listed in Table 1. The x and z coordinate values for the Sun are not exactly zero for these cases as the solar system baryonic centre does not lie on either the Sun-Jupiter axis or the Sun-Neptune axis. The resulting position, (x_o, y_o, z_o) , of the saddle point for both the Sun-Jupiter pair and the Sun-Neptune pair, plus the resulting values of y_{op} , are included in the Table. As is seen by the values of y_{op} , the position of the saddle point hosted by both Jupiter and Neptune is in the outer regions of their satellite systems.

A major source of uncertainty in the location of the saddle point for both the Sun-Jupiter and the Sun-Neptune systems arises from the uncertainty in the gravitational parameter for the given planets. The uncertainty of ±1.5 km³ s⁻² for the gravitational parameter of Jupiter leads to an uncertainty of ±135 m for its corresponding y_o and y_{op} values, while the uncertainty of ±10 km³ s⁻² for the gravitational parameter of Neptune leads to a corresponding uncertainty of ±23.2 km for its corresponding y_o and y_{op} values. These uncertainties give an estimate of how accurately the saddle point position could be determined for these two-body systems. There are also uncertainties from massive satellites, which we discuss later in Sect. 3.4.

3.2 Size

Of course, the size of the saddle region where $g < \delta_g$, is of great importance given that an experiment is to be carried out within that region. With respect to a coordinate system (x', y', z') , where the origin is at the saddle point and the y' axis lies along the Sun-planet axis, the net gravitational field magnitude about the saddle point is given by

$$g = |\mathbf{g}_\odot + \mathbf{g}_p| \tag{32a}$$

$$= GM_p \left[\frac{x'^2 + z'^2}{(x'^2 + z'^2 + (y_{op} - y')^2)^3} + \left(\frac{y_{op} - y'}{(x'^2 + z'^2 + (y_{op} - y')^2)^{3/2}} - \frac{1}{y_{op}^2} \right)^2 \right]^{1/2} \tag{32b}$$

where the substitution for g_\odot from (31) has been used. Using the values as given in Table 1, the net gravitational field within the saddle region, using (32b), was determined for both the Sun-Jupiter and Sun-Neptune systems. The resulting gravitational field profiles for both these system are shown in Fig. 2. To first order, with x', y' and $z' \ll y_{op}$, (32b) reduces to

$$g \cong \frac{GM_p}{y_{op}^3} (x'^2 + z'^2 + (2y')^2)^{1/2}, \tag{33}$$

the equation for an ellipsoid.

Setting $g = \delta_g$ in (33), the width, Δw_{sp} , of the saddle region along the y' axis and the diameter, Δd_{sp} , of the saddle region perpendicular to y' are, to first order, given by

$$\Delta w_{sp} \cong \frac{y_{op}^3}{GM_p} \delta_g \tag{34}$$

and

$$\Delta d_{sp} \cong \frac{2y_{op}^3}{GM_p} \delta_g \tag{35}$$

respectively. For this manuscript, δ_g will be taken to be $1.00 \times 10^{-10} \text{ ms}^{-2}$, i.e. within the saddle region the magnitude of the gravitational field is $< 1.00 \times 10^{-10} \text{ ms}^{-2}$, which is about the same as g_\odot , the fundamental acceleration scale in MOND and GRAS. For this value of δ_g the first order values of Δw_{sp} and Δd_{sp} , from (34) and (35), are 10.2 km and 20.3 km for the saddle region hosted by Jupiter and 475 km and 950 km for the saddle region hosted by Neptune, in good agreement with Fig. 2. The sizes of these saddle regions are therefore of reasonable extent in which to carry out an experiment.

To gain a better understanding of the factors that determine the size of a saddle region, the approximation that for $y_{op} \ll R$

$$g_\odot \cong \frac{GM_\odot}{R^2} \tag{36a}$$

will be used, and, therefore, by (31)

$$y_{op} \cong \left(\frac{M_p}{M_\odot} \right)^{\frac{1}{2}} R. \tag{36b}$$

By (34) and (36b), along with a value of $\delta_g = 1.00 \times 10^{-10} \text{ ms}^{-2}$, the size of a saddle region can be expressed as

$$\Delta w_{sp} \cong \frac{\delta_g}{GM_\odot^{3/2}} (M_p^{1/2} R^3) \tag{37a}$$

$$\cong 4.37m (M_p^{1/2} R^3) \tag{37b}$$

and

$$\Delta d_{sp} \cong \frac{2\delta_g}{GM_\odot^{3/2}} (M_p^{1/2} R^3) \tag{38a}$$

$$\cong 8.74m (M_p^{1/2} R^3) \tag{38b}$$

where M'_p is in units of M_\oplus and R' is in AU. As (37b) and (38b) show, the greater the mass of the host planet and the weaker the gravitational field due to the Sun, i.e. the greater R , the larger the saddle region. Hence the necessity of using saddle regions hosted by the larger outer solar system planets. For example, in the case of Earth, (37b) leads to a value of 4.37 m for Δw_{sp} . Only the saddle regions that are hosted by the larger outer solar system planets are large enough to be viable locations for the proposed experiment.

3.3 Availability

A given saddle region will travel through space in sync with its host planet in orbit about the centre of mass of the two-body system, in our case taken to be the solar system barycentre. In the case of the planet being in circular orbit, the speed of the saddle point about the mass centre will be given by

$$v_{sp} = \frac{y_o}{R} \left(\frac{GM_\odot}{y_o} \right)^{\frac{1}{2}}. \tag{39}$$

Within a given saddle region the gravitational field is $\leq 1.00 \times 10^{-10} \text{ m s}^{-2}$. Therefore, any passive body within a saddle region will travel, for all intents and purposes, at constant velocity with respect to an inertial reference frame. Figure 3 shows the resulting path of a passive body traveling through a saddle region.

Fig. 2 The gravitational field profile of the saddle region hosted by (a) Jupiter and (b) Neptune. The solid line corresponds to a value of $1.00 \times 10^{-10} \text{ ms}^{-2}$ and dashed line corresponds to a value of $5.00 \times 10^{-11} \text{ ms}^{-2}$. The arrows indicate the direction of the gravitational field

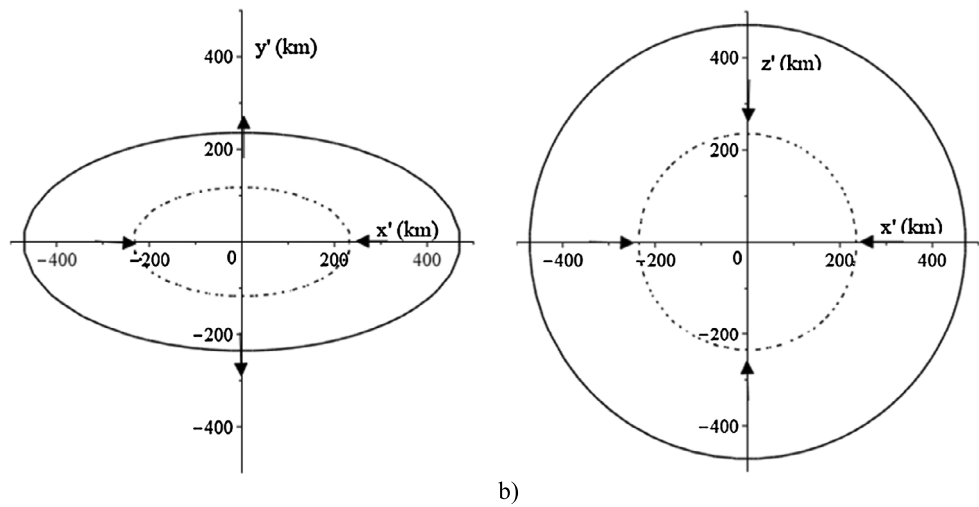
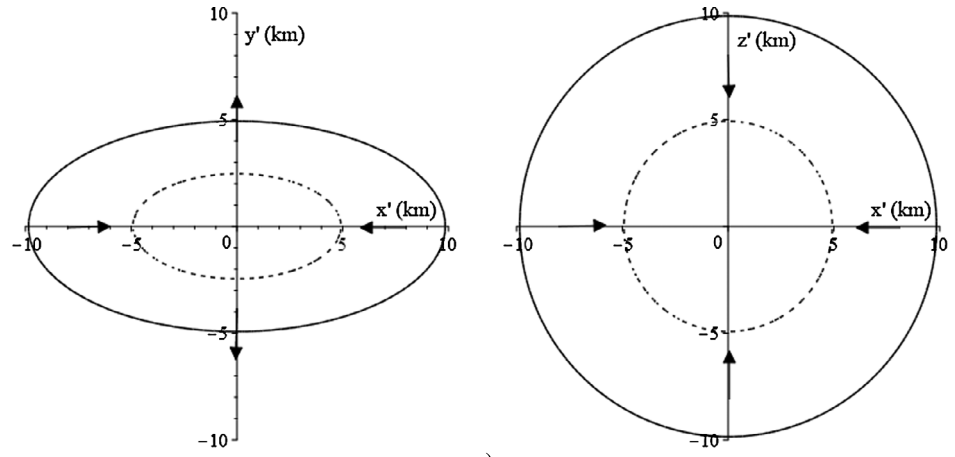


Fig. 3 The path of a passive body through a saddle region (not to scale). The arrows indicate the gravitational field acting on the passive body at the different locations

For circular orbits, and using (39), it can be shown that the maximum time that a coasting body could remain in a saddle region, corresponding to the path shown in Fig. 3, is given, to first order, by

$$\Delta t_{sp} \cong \frac{1}{GM_p} \left(8\delta_g y_{op}^5 \right)^{1/2} \tag{40}$$

For a value of $1.00 \times 10^{-10} \text{ ms}^{-2}$ for δ_g , the resulting values of Δt_{sp} for Jupiter and Neptune are $1.88 \times 10^4 \text{ s}$ (5.22 hours) and $7.53 \times 10^5 \text{ s}$ (209 hours) respectively. These are reasonable times over which to carry out an experiment. Given that the orbits of planets are elliptical, (40) should be taken to be the average over an orbit. However, as both Jupiter and Nep-

tune have rather low orbital eccentricities of 0.048 and 0.009 respectively, the variation in times will be relatively small. With the approximation as given by (36b), it follows from (40) that

$$\Delta t_{sp} \cong (77 \text{ s}) M_p'^{1/4} R'^{5/2} \tag{41}$$

Eq. (41) shows again the necessity of using the saddle regions hosted by the larger outer solar system planets. For the Earth (41) leads to $\Delta t_{sp} = 77 \text{ s}$. For a typical acceleration scale of $a = 10^{-10} \text{ ms}^{-2}$ this would lead to a displacement on the order of only several hundred nm, shorter than the wavelength of a visible photon. Therefore, a more mas-

Table 2 The contributors to g_{EXT} , for both the Jupiter and Neptune hosted saddle points, whose gravitational field magnitude is greater than $1.0 \times 10^{-12} \text{ ms}^{-2}$ at the reference time of Jan 01-2020-00.00.0000. The bracketed numbers represent the uncertainties

Body	g_{BODY} at Jupiter s.p. $\times 10^{-12} \text{ ms}^{-2}$	g_{BODY} at Neptune s.p. $\times 10^{-12} \text{ ms}^{-2}$
Galaxy	217	217
Sun	326144695	9494801
Mercury	65	2
Venus	785	24
Earth	688	28
-Moon	8	
Mars	128	3
Jupiter	326011748	9757
-Ganymede	24639 (17)	
-Io	14961 (25)	
-Europa	8243 (26)	
-Calisto	16602 (15)	
Saturn	77140	3611
-Titan	18	
Uranus	597	676
Neptune	373	9506590 (14)
-Triton		2027 (14)
-Proteus		5
-Nereid		3

sive and/or distant planet is required for the proposed experiment.

3.4 Effect of other solar system bodies and the Galaxy

The size of a saddle region is determined primarily by the gradient of the host planet’s gravitational field. In the case of the other solar system bodies, as well as for the Galaxy, their gravitational fields at a given time can, to a good approximation, be taken to be constant over the extent of a given saddle region. Therefore, these other bodies will not have a significant effect on the size of the saddle region.

However, these other bodies will have a very significant effect on the location of the saddle point. Taking that the system is now comprised of all the solar system bodies plus the Galaxy, the net gravitational field at the new saddle point location will be given by

$$\mathbf{g} = \mathbf{g}_{\odot} + \mathbf{g}_{\text{p}} + \mathbf{g}_{\text{Galaxy}} + \Sigma \mathbf{g}_{\text{ss}} \tag{42}$$

where $\mathbf{g}_{\text{Galaxy}}$ is the gravitational contribution of the Galaxy, and $\Sigma \mathbf{g}_{\text{ss}}$ is the contribution of all the other solar system bodies, i.e. besides the Sun and Jupiter or the Sun and Neptune. Table 2 lists the primary contributors to \mathbf{g} at the saddle point hosted by both Jupiter and Neptune at the reference time of Jan 01-2020-00.00.0000. These contributors

include the Galaxy and those solar system bodies whose gravitational field magnitude is greater than 10^{-12} ms^{-2} at the given saddle point location and time. In the case of $\mathbf{g}_{\odot} + \mathbf{g}_{\text{p}} + \Sigma \mathbf{g}_{\text{ss}}$, the positional values of the solar system bodies listed in Table 2 on Jan 01-2020-00.00.0000, as taken from <https://ssd.jpl.nasa.gov/?horizons>, were used to determine each of their individual contributions.

To provide an estimate for $\mathbf{g}_{\text{Galaxy}}$, it will be approximated that the solar system is in circular orbit about the Galactic centre in a fixed plane. Taking the Sun to be 8.122 kpc from the galactic centre and orbiting at a speed of 233.3 km s^{-1} (McGaugh 2018) the resulting estimate for g_{Galaxy} is therefore $2.17 \times 10^{-10} \text{ ms}^{-2}$. Given that Banik and Zhao (2018) estimated the impact of the disc on the galactic gravitational field at the Sun’s location to be only 1.9 per cent, neglecting the effect of the disc is reasonable. As the angle between the galactic plane and the planetary orbit plane is approximately 60° , the z -component of Galaxy’s contribution will be approximately $g_{\text{Galaxy}} \sin 60^{\circ}$. For this example, it will be taken that the Galaxy’s x and y gravitational components are equal in magnitude, which corresponds to their average values over a given planet’s orbit. Although the value of $\mathbf{g}_{\text{Galaxy}}$ at the specific reference time is what is required, this does provide an estimate of the Galaxy’s contribution to \mathbf{g} at the saddle point.

In Table 3 are listed the positions of the saddle points, (x_{o+}, y_{o+}, z_{o+}) , taking into account the contributors listed in Table 2. The overall effect of the contributors, other than the Sun and gas planet, is to shift the saddle point hosted by Jupiter by $5.60 \times 10^3 \text{ km}$ and the saddle point hosted by Neptune by $2.12 \times 10^4 \text{ km}$. In the case of the saddle point hosted by Jupiter 99.7% of the shift is due to the combined gravitational fields of Saturn and Jupiter’s four large moons. In the case of the saddle point hosted by Neptune 99.0% of the shift is due to the combined gravitational fields of Jupiter, Saturn, and Triton. Of course, this will be dependent on the specific reference time.

The accuracy for which a given saddle point can be located at a specific time is dependent on the precision to which \mathbf{g} at the saddle point is known. For example, if g is known to a precision of 10^{-10} ms^{-2} the position of the saddle point will be known to the accuracy as shown by the 10^{-10} ms^{-2} contours in Fig. 2. The uncertainties in the individual contributions shown in Table 2 are due to the uncertainty in the value of GM for Neptune and the uncertainty in the masses of the Jovian moons and Triton as provided by <https://ssd.jpl.nasa.gov/?horizons>. Adding in quadrature the uncertainties in g , as listed in Table 2, indicates that the value of g at the saddle point hosted by Jupiter is known to a precision of $\sim 5.6 \times 10^{-11} \text{ ms}^{-2}$. This corresponds to knowing the location of the saddle point hosted by Jupiter to within $\pm 2.8 \text{ km}$ along y' and $\pm 5.7 \text{ km}$ along x' and z' , i.e. approximately within the $5 \times 10^{-11} \text{ ms}^{-2}$ contour

Table 3 The position and uncertainties of the saddle points hosted by Jupiter and Neptune considering all the bodies listed in Table 2, (x_{o+}, y_{o+}, z_{o+}) . Included are the Δw_{sp} and Δd_{sp} sizes of the corresponding saddle regions as well as Δt_{sp} , the maximum time that a passive body could remain in the saddle region

	Jupiter s.p.	Neptune s.p
x_{o+}	0.0000700223 AU (10, 475.2 ± 5.7) km	0.00001007 AU (1506 ± 95) km
y_{o+}	5.0630893475 AU (757, 427, 387.1 ± 2.8) km	29.71444274 AU (4, 445, 217, 372 ± 47) km
z_{o+}	0.0000011650 AU (174.3 ± 5.7) km	0.00000643 AU (962 ± 95) km
Δw_{sp}	10.2 km	475 km
Δd_{sp}	20.3 km	950 km
Δt_{sp}	1.88×10^4 s = 5.22 h	7.53×10^5 s = 209 h

shown in Fig. 2a. In the case of Neptune, it would appear that g at that saddle point can be known to a precision of $\sim 2.0 \times 10^{-11} \text{ ms}^{-2}$. This corresponds to knowing the location of the saddle point hosted by Neptune to within ± 47 km along y' and ± 95 km along x' and z' . These values are included in Table 3. The primary reason for these relatively small uncertainties in saddle point position is that the masses of Triton and the Galilean moons of Jupiter are known to rather high precision due to spacecraft flybys. Although these estimates may be overly optimistic, in both cases the uncertainty in the position of the saddle points lies well within the saddle regions being considered for the experiment. It is further hoped that measurements taken prior to or during the mission itself would significantly reduce these uncertainties.

One body which has not been included in Table 2, is the hypothetical Planet 9. There is indirect observational evidence of a planet with a mass between $\sim 5\text{--}20M_{\oplus}$, on an eccentric and inclined orbit with an approximate perihelion of ~ 250 AU (Batygin and Brown 2016; Bailey et al. 2016). If it did exist, its contribution to g at the saddle points would be $< 6 \times 10^{-12} \text{ ms}^{-2}$ and therefore would involve a relatively small shift in the saddle point positions.

During the experiment the positions of solar system bodies will change. Although the effect will be relatively small, the true path of the saddle point over the duration of the experiment, taking into account this motion, would need to be determined. Also, the SSB centred coordinate system is not an inertial reference frame as the origin of this reference system revolves around the Galactic centre. In the reference frame where the origin is at the centre of the Galaxy, taken to be an inertial reference system, a passive body will move through a saddle region in a straight line. With respect to the SSB centred coordinate system the motion of a passive body through a saddle region will not be a straight line but will appear to accelerate at $2.17 \times 10^{-10} \text{ ms}^{-2}$ away from

the galactic centre. In the case of a passive body coasting through the saddle region hosted by Jupiter, over the time $\Delta t_{sp} = 1.88 \times 10^4$ s this will result in the body shifting away from the Galactic centre by approximately 3.8 cm. The impact of the motion of the Galactic centre within the Local group would be very much smaller. The motion of the saddle point is thus mainly determined by planetary orbital motion within the Solar System. The Galaxy does affect the saddle point location, but its shift due to the Galactic gravity would be known in advance since we know g_{Galaxy} .

4 Experiment

For the proposed experiment, it will be taken that it is carried out in the saddle region hosted by Jupiter. This experiment will require that a spherically symmetric body of mass $M_1 = 100$ kg and radius $r_1 = 30.0$ cm be brought to Jupiter by a spacecraft. For our example, it will be taken that the true path of the saddle point is as given by Fig. 3. In this case, the spacecraft would be placed in orbit around Jupiter such that at its apogee it would be at the position A shown in Fig. 3, and travelling with a speed matching that of the saddle region. With respect to Jupiter this speed would be approximately 397 ms^{-1} as determined, using (39), by

$$v_{sp,J} = \left(1 - \frac{y_o}{R}\right) \left(\frac{GM_{\odot}}{y_o}\right)^{\frac{1}{2}} \tag{43}$$

At the instant that the spacecraft's velocity is in the direction \vec{AE} as shown in Fig. 3, the 100 kg body would be released and the spacecraft would then leave the saddle region. After being released the body would then place, with a telescopic arm or by some other means, a second spherically symmetric body, parallel to the x' axis at a distance of 6.00 m from the centre of M_1 . This second body will be taken to have a mass of $M_2 = 2.00$ kg and a radius of $r_2 = 4.24$ cm. The masses and radii are chosen so that both masses are equally affected by Solar radiation pressure (45). The relative separation of M_1 and M_2 would then be tracked, either by interferometry or by the time-of-flight of a reflected laser pulse, as the two masses coast through the saddle region. The two masses would remain within the saddle region for a time of $\Delta t_{sp} = 1.88 \times 10^4$ s. As will be shown, this experiment will lead to very definitive results.

At a distance of 6.00 m the Newtonian gravitational field at M_2 due to M_1 would be $1.85 \times 10^{-10} \text{ ms}^{-2}$ while that at M_1 due to M_2 would be $3.71 \times 10^{-12} \text{ ms}^{-2}$. The Newtonian relative acceleration between the two masses would therefore be $1.89 \times 10^{-10} \text{ ms}^{-2} = 1.58g_o$, which is slightly smaller than g_{Galaxy} . According to MOND and GRAS however the gravitational fields generated by the two masses would be greater. Treating initially that the two masses are

independent of each other, and using (26), the gravitational field at a distance of 6.00 m from M_1 and M_2 would be $2.45 \times 10^{-10} \text{ ms}^{-2}$ and $2.26 \times 10^{-11} \text{ ms}^{-2}$ respectively. The relative acceleration between the two masses would then be $2.68 \times 10^{-10} \text{ ms}^{-2}$, significantly greater than the Newtonian value. Figure 4 shows the resulting mass dipole moment density profile surrounding the isolated M_1 . As is seen, the mass dipole moment density goes to zero in the relatively strong gravitational field near M_1 . Again, GRAS is different from other mass dipole theories where the mass dipole moment density saturates in strong fields. Figure 5 shows the resulting mass density distribution, due to the mass dipoles, and the net gravitational field around the isolated M_1 . At distances $\gtrsim 6$ m, the mass density distribution begins to fall off as r^{-2} while the gravitational field falls off as r^{-1} . The BTFR value for the isolated M_1 is $2.99 \times 10^{-5} \text{ ms}^{-1}$. In the case of MOND the mass density distribution shown in Fig. 5a) would correspond to the phantom dark matter density of (12).

According to GRAS, the increased gravitational fields around both M_1 and M_2 are due to their surrounding mass dipole distributions. This distribution depends on the total gravitational field and as such M_1 and M_2 cannot be treated as independent of each other as the surrounding mass dipole distribution will be altered when the two masses are placed near each other. Using the method of Sect. 2.3, Fig. 6 shows the resulting surrounding mass density distribution and the net gravitational field in the case where M_1 and M_2 are 6.00 m apart. Due to the large mass difference between M_1 and M_2 , the effect on the gravitational field at M_2 due to M_1 is relatively small, and drops only slightly from $2.45 \times 10^{-10} \text{ ms}^{-2}$ to $2.43 \times 10^{-10} \text{ ms}^{-2}$. The effect on the gravitational field at M_1 due to M_2 is however significant as its magnitude drops from $2.26 \times 10^{-11} \text{ ms}^{-2}$, in the case of no interaction, to $4.87 \times 10^{-12} \text{ ms}^{-2}$, approximately 30% greater than just its baryonic mass contribution. The relative acceleration between M_1 and M_2 will now be $2.48 \times 10^{-10} \text{ ms}^{-2}$, corresponding to approximately a 7.5% drop from the case where there is no interaction. If the mass difference was not so large the overall impact would be even greater. For example, when considering binary galaxies (Penner 2017), in the case where the masses of the two galaxies are equal, the distortion of the mass density distribution led to a drop in the gravitational field at each others location of approximately 25%.

In addition to the changes to the mass dipole distribution due to the interaction of the two masses, the effect that the external gravitational field has on the dipole distribution needs to be considered. The external gravitational field will be the gravitational field within the saddle region due to the Sun, Jupiter, other solar system bodies, and the Galaxy, i.e. the contributors listed in Table 2. As Fig. 3 indicates, to a good approximation the external gravitational field acts

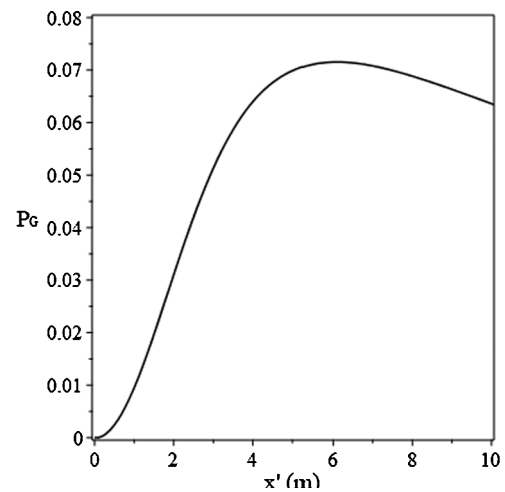


Fig. 4 The mass dipole moment density, P_G , surrounding the mass M_1 . The units for P_G are kg m^{-2}

along the y' axis as the two bodies travel from position A to E. The maximum value of g_{EXT} during the transversal will be $1.00 \times 10^{-10} \text{ ms}^{-2}$ which will occur at points A, C, and E, while the minimum value of g_{EXT} will be 0 ms^{-2} which will occur at points B and D. Over the dimensions of the experiment, i.e. 6.00 m, the external gravitational field will to be taken to be constant at any given time during the transversal.

Ideally, the effects on the mass dipole distribution due to the interaction of the two masses and those due to the external gravitational field would be determined together. However, as the two masses are moving parallel to the x' axis while the external gravitational field is along the y' axis, the problem is not axisymmetric. As such, the two effects were handled separately, on the provision that the individual impacts of the two effects are relatively small. Using the method of Sect. 2.3, Fig. 7a shows the effect that a constant external field of magnitude $1.00 \times 10^{-10} \text{ ms}^{-2}$ acting along y' has on the mass density distribution surrounding M_1 . As is seen, the effect is dramatic. Beyond 5 m the mass density due to the mass dipole distribution falls rapidly. The impact on the gravitational field is shown in Fig. 7b. By comparing the outer contour lines of Fig. 5b and Fig. 7b, it can be seen that the constant external field ends up reducing the net gravitational field, although slightly. At a distance of 6.00 m from M_1 along the x' axis the gravitational field, as a result of the external field, drops from $2.45 \times 10^{-10} \text{ ms}^{-2}$ to $2.41 \times 10^{-10} \text{ ms}^{-2}$, a decrease of 1.2%. However, the magnitude of this drop will be the maximum, occurring at points A, C, and E. At points B and D, as g_{EXT} is equal to zero, there will be no drop in the gravitational field due to M_1 . By approximating that the magnitude of g_{EXT} changes linearly as the bodies travel from point A to E, the average effect of g_{EXT} would be to reduce the gravitational field of M_1 at 6.00 m by 0.6%. Neglecting the impact of g_{EXT} on the

Fig. 5 (a) The mass density distribution surrounding an isolated M_1 . The thick solid line corresponds to 0.05 kg m^{-3} and the thin solid line corresponds to 0.02 kg m^{-3} . (b) The gravitational field surrounding M_1 . The thick solid line corresponds to $5.0 \times 10^{-10} \text{ ms}^{-2}$ and the thin solid line corresponds to $2.0 \times 10^{-10} \text{ ms}^{-2}$

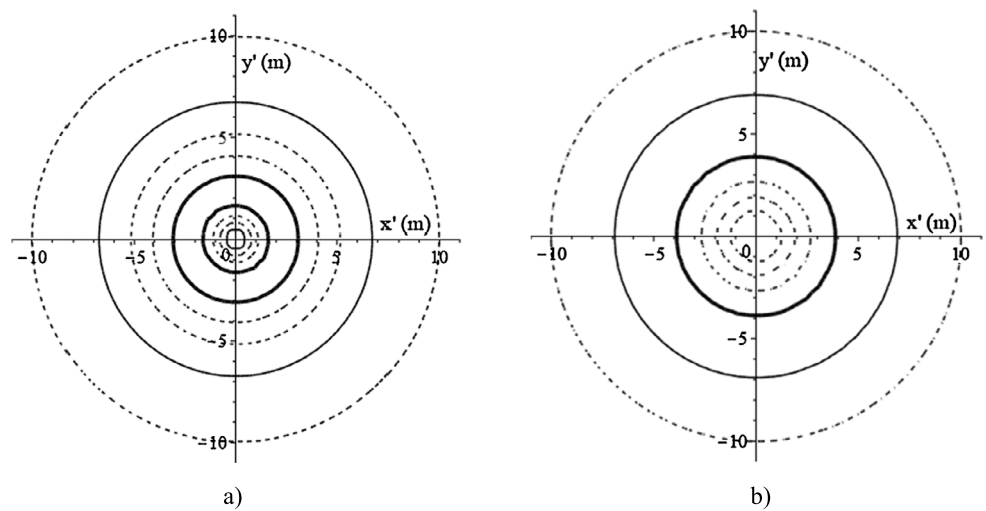
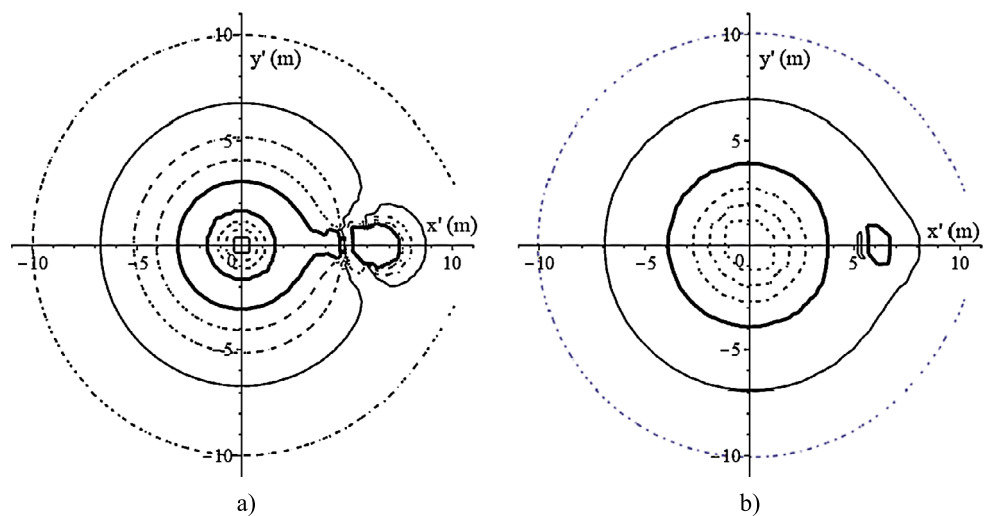


Fig. 6 (a) The mass density distribution surrounding M_1 and M_2 . The thick solid line corresponds to 0.05 kg m^{-3} and the thin solid line corresponds to 0.02 kg m^{-3} . (b) The gravitational field surrounding M_1 and M_2 . The thick solid line corresponds to $5.0 \times 10^{-10} \text{ ms}^{-2}$ and the thin solid line corresponds to $2.0 \times 10^{-10} \text{ ms}^{-2}$



gravitational field at M_1 due to M_2 , the resulting relative acceleration between the two masses will therefore decrease from $2.48 \times 10^{-10} \text{ ms}^{-2}$ to $2.44 \times 10^{-10} \text{ ms}^{-2}$.

In addition to the motion along x' , as a result of the external field the two masses will also accelerate along the y' axis. In the Newtonian case, both masses would experience the same acceleration along the y' axis, i.e. at point A both would experience an acceleration of $1.00 \times 10^{-10} \text{ ms}^{-2}$ (in Fig. 7b this has been subtracted out). In the case of GRAS and MOND, which are non-linear theories, the accelerations along y' of M_1 and M_2 will, in general, not be the same. The difference between the two can be approximated by considering the additional transverse component of the gravitational field due to M_1 at the location of M_2 . This shows up in Fig. 7b where it can be seen that the gravitational field surrounding M_1 is no longer spherically symmetric, as indicated by the shift in the outer contours. For the given experimental setup, the additional transverse component of the gravitational field at the location of M_2 is found to be

$< 10^{-12} \text{ ms}^{-2}$. Compared to the motion along x' , the effect is therefore negligible.

With regards to the method of solution, as outlined in Sect. 2.3, for Figs. 5 through 7, the region of space considered for the computation was a sphere of radius 11.0 m centred on M_1 , divided into rings of width and thickness of 0.100 m. For this ring size the values of g generated throughout the spherical region for Fig. 5b were within 0.05% of the values calculated using (26) after only 5 iterations. For Figs. 6 and 7 convergence was again fairly rapid with variations in the value of g throughout the region being $< 0.1\%$ after 10 iterations.

The relative acceleration between M_1 and M_2 of $2.44 \times 10^{-10} \text{ ms}^{-2}$ is based on the function as given by (24). This function led to a good fit to the RAR and agreed with observations within the solar system. Ideally an even better fitting function to the RAR would be found. At a value of $g = 2.44 \times 10^{-10} \text{ ms}^{-2}$, (26) leads to a value of $1.84 \times 10^{-10} \text{ ms}^{-2}$ for g_N . Substituting this value for g_N into the RAR (1), then leads to a value of $g = 2.59 \times 10^{-10} \text{ ms}^{-2}$.

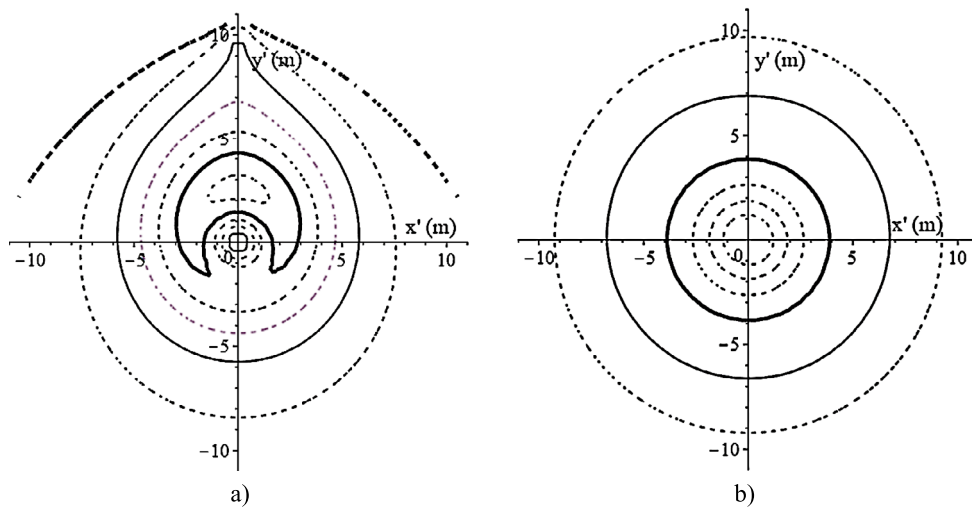


Fig. 7 (a) The mass density distribution surrounding M_1 with a constant external gravitational field of $1.00 \times 10^{-10} \text{ ms}^{-2}$ pointing along the y' axis. The thick solid line corresponds to 0.05 kg m^{-3} and the thin solid line corresponds to 0.02 kg m^{-3} . The thick dashed line cor-

responds to 0.00 kg m^{-3} . (b) The gravitational field surrounding M_1 . The thick solid line corresponds to $5.0 \times 10^{-10} \text{ ms}^{-2}$ and the thin solid line corresponds to $2.0 \times 10^{-10} \text{ ms}^{-2}$. The constant external gravitational field of $1.00 \times 10^{-10} \text{ ms}^{-2}$ has been subtracted out

It would therefore be expected that a better fitting function to the RAR would lead to a relative acceleration between M_1 and M_2 of $2.59 \times 10^{-10} \text{ ms}^{-2}$. This is the prediction of GRAS and MOND.

There is also a nongravitational force that needs to be considered, and the reason why M_2 is placed along the x' axis. The solar radiation pressure at the location of Jupiter’s saddle point is given by

$$P_{srp} = 4.57 \times 10^{-6} \text{ Nm}^{-2} \left(\frac{R_{\oplus}}{y_o} \right)^2 \tag{44a}$$

$$= 1.78 \times 10^{-7} \text{ Nm}^{-2}. \tag{44b}$$

The resulting acceleration, a_{srp} , of a perfect reflector of mass M and cross-sectional A will therefore be

$$a_{srp} = 2(1.78 \times 10^{-7} \text{ Nm}^{-2}) \frac{A}{M}. \tag{45}$$

For the given radii of M_1 and M_2 , i.e. 30.0 cm and 4.24 cm, the ratio A/M is equal $2.83 \times 10^{-3} \text{ m}^2 \text{ kg}^{-1}$ for both masses, so they will therefore have exactly the same $a_{srp} = 1.01 \times 10^{-9} \text{ ms}^{-2}$. The solar radiation pressure will therefore not affect the relative separation of M_1 and M_2 . Due to the solar radiation pressure both masses will drift a distance of 17.8 cm in a direction away from the Sun over a time of $\Delta t_{sp} = 1.88 \times 10^4 \text{ s}$.

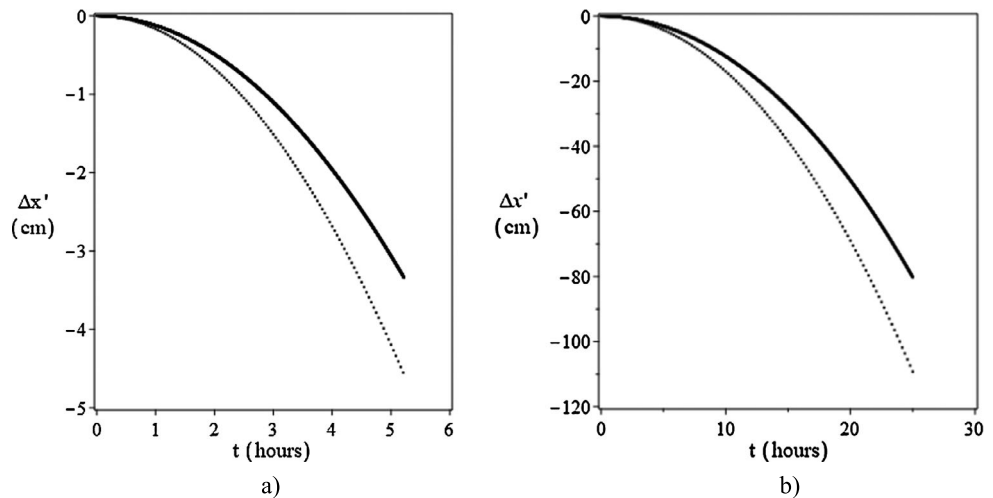
Figure 8a shows the change in the separation of M_1 and M_2 for the Newtonian relative acceleration of $1.89 \times 10^{-10} \text{ ms}^{-2}$ and the GRAS and MOND prediction of $2.59 \times 10^{-10} \text{ ms}^{-2}$. In a time of $1.88 \times 10^4 \text{ s}$ the relative separation of M_1 and M_2 would decrease by 3.34 cm in the Newtonian case and 4.58 cm in the GRAS and MOND case. The difference of 1.24 cm would be easily measured.

In the case of the Jupiter hosted saddle region, the RAR relative acceleration between M_1 and M_2 corresponds to a value of $g_N = 1.84 \times 10^{-10} \text{ ms}^{-2}$, which to a good approximation is equal to the value of g_N at the location of M_2 due to M_1 , i.e. $1.85 \times 10^{-10} \text{ ms}^{-2}$. Taking this result to hold as the relative separation of M_1 and M_2 continues to decrease, one can extrapolate to the case where the experiment is carried out in the saddle region hosted by Neptune, where Δt_{sp} is much greater. The result is shown in Fig. 8b. After 25 hours, the difference between the Newtonian case and the GRAS and MOND case is 29.0 cm. Overall, the saddle region hosted by Neptune is superior to that hosted by Jupiter for any such experiment. Not only does the greater Δt_{sp} lead to greater differences between the Newtonian case and the GRAS and MOND case, the relative uncertainty in the saddle point location is also less, and the solar radiation pressure would be significantly less. However, Jupiter is significantly closer and the difference of over 1 cm between Newtonian theory and the theories of GRAS and MOND would be easily detectable, so Jupiter is more than adequate for the experiment. Which ever gas planet hosted saddle region is used the results of the experiment would be quite definitive. Ideally the mass M_2 could be retrieved and experiment could be repeated with different initial starting separations and even different orientations. Also, it would be hoped that the host spacecraft would track M_1 during the experiment, if only to verify that the experiment is run in a saddle region.

5 Conclusion

Sun-gas planet saddle regions provide the opportunity to test gravitational theory in the realm of field strengths which cor-

Fig. 8 The separation of M_1 and M_2 over the duration of the experiment carried out in the saddle region hosted by (a) Jupiter and (b) Neptune. The solid line corresponds to the expected Newtonian result. The dotted line corresponds to the prediction of GRAS and MOND



respond to that found in the outer regions of galaxies. As the manuscript has demonstrated these saddle regions are large enough and available long enough in order to carry out experiments. The more massive and the further from the Sun the gas planet, the larger its saddle region and the longer it is available for any experiment. As such the Neptune hosted saddle region is the most attractive. However, the relative closeness of Jupiter, makes its saddle region also attractive. The experiment outlined in this manuscript would seem to be the most direct way to test the different gravitational theories, however, there certainly may be better ways that testing could be carried out. The theories of MOND and GRAS give very definite predictions with regards to the proposed experiment. When carrying out the experiment in the saddle region hosted by Jupiter the final difference between the average separation of the two masses corresponding to Newtonian theory and the theories of GRAS and MOND will exceed 1 cm. In the case of the saddle region hosted by Neptune, depending on the length of time the experiment is run, differences will greatly exceed 10 cm. This result is independent of the specific formulation of MOND as all formulations must lead to agreement with the RAR and the BTFR. Indeed, any alternative gravitational theory which agrees with the RAR and the BTFR will lead to this result.

A positive result would certainly indicate that the dark matter explanation for the various astronomical explanations is incorrect. The current alternative theories, plus the multitude that would arise after a positive result, would all vie for the being the replacement theory. Ideally a theory of quantum gravity would come forth that would lead to the RAR and the BTFR. The theory of GRAS may provide a clue as to how this could happen. Conversely, a null result would eliminate GRAS and MOND as possibilities and would add support to the theory of dark matter. The key is that the opportunity to know which road to take in order to understand current astronomical observations does exist!

Publisher's Note Springer Nature remains neutral with regard to jurisdictional claims in published maps and institutional affiliations.

References

- Bailey, E., Batygin, K., Brown, M.E.: *Astron. J.* **152**, 126 (2016)
- Banik, I., Kroupa, P.: *Mon. Not. R. Astron. Soc.* **487**, 2665 (2019)
- Banik, I., Kroupa, P.: *Mon. Not. R. Astron. Soc.* **495**, 3974 (2020)
- Banik, I., Zhao, H.: *Mon. Not. R. Astron. Soc.* **480**, 2660 (2018)
- Batygin, K., Brown, M.E.: *Astron. J.* **151**, 22 (2016)
- Bekenstein, J.D., Magueijo, J.: *Phys. Rev. D* **73**, 103513 (2006)
- Bekenstein, J.D., Milgrom, M.: *Astrophys. J.* **286**, 7 (1984)
- Bevis, N., Magueijo, J., Trenkel, C., Kembler, S.: *Class. Quantum Gravity* **27**, 215014 (2010)
- Blanchet, L.: *Class. Quantum Gravity* **24**, 3529 (2007a). [astro-ph/0605637](https://arxiv.org/abs/astro-ph/0605637)
- Blanchet, L.: *Class. Quantum Gravity* **24**, 3541 (2007b). [gr-qc/0609121](https://arxiv.org/abs/gr-qc/0609121)
- Blanchet, L., LeTiec, A.: (2008). [http://arXiv.org/abs/0804.3518](https://arxiv.org/abs/http://arXiv.org/abs/0804.3518)
- Bondi, H.: *Rev. Mod. Phys.* **29**(3), 423 (1957).
- Debono, I., Smoot, G.F.: *Universe* **2**(4), 23 (2016)
- Famaey, B., McGaugh, S.: *Living Rev. Relativ.* **15**, 10 (2012)
- Galianni, P., Feix, M., Zhao, H., Horne, K.: *Phys. Rev. D* **86**, 044002 (2012)
- Hajdukovic, D.S.: *Astrophys. Space Sci.* **334**, 215 (2011a)
- Hajdukovic, D.S.: *Adv. Astron.* **196**, 852 (2011b)
- Hajdukovic, D.S.: *Mod. Phys. Lett. A* **26**, 1555 (2011c)
- Hajdukovic, D.S.: *Astrophys. Space Sci.* **337**, 9 (2012a)
- Hajdukovic, D.S.: *Astrophys. Space Sci.* **339**(1), 1 (2012b).
- Hajdukovic, D.S.: *Astrophys. Space Sci.* **343**, 505 (2013)
- Iorio, L.: *Open Astron. J.* **3**, 156 (2010a)
- Iorio, L.: *Open Astron. J.* **3**, 1 (2010b)
- Iorio, L.: *Universe* **1**(1), 38 (2015)
- Iorio, L.: *Astrophys. Space Sci.* **364**, 126 (2019)
- Magueijo, J., Mozaffari, A.: *Phys. Rev. D* **85**, 043527 (2012).
- Magueijo, J., Mozaffari, A.: *Class. Quantum Gravity* **30**, 9 (2013)
- McGaugh, S.S.: *RNAAS* **2**(3) (2018)
- McGaugh, S.S., Lelli, F., Schombert, J.M.: *Phys. Rev. Lett.* **117**, 201101 (2016)
- Milgrom, M.: *Astrophys. J.* **270**, 365 (1983a)
- Milgrom, M.: *Astrophys. J.* **270**, 371 (1983b)
- Milgrom, M.: *Astrophys. J.* **270**, 384 (1983c)
- Milgrom, M.: *Mon. Not. R. Astron. Soc.* **403**, 886 (2010)

- Paučo, R., Klačka, J.: *Astron. Astrophys.* **589**, A63 (2016)
- Penner, A.R.: *Astrophys. Space Sci.* **361**, 124 (2016a)
- Penner, A.R.: *Astrophys. Space Sci.* **361**, 361 (2016b)
- Penner, A.R.: *Astrophys. Space Sci.* **362**, 80 (2017)
- Penner, A.R.: Gravitational anti-screening as an alternative to dark matter. In: Mehler, N. (ed.) *Research Advances in Astronomy*, pp. 1-48. Nova US, New York, NY (2018)
- Penner, A.R.: *Astrophys. Space Sci.* **365**, 65 (2020)
- Pitjev, N.P., Pitjeva, E.V.: *Astron. Lett.* **39**(3), 141 (2013)
- Pittordis, C., Sutherland, W.: (2019). [arXiv:1905.09619](https://arxiv.org/abs/1905.09619)
- Sanders, R.H.: *Can. J. Phys.* **93**(2), 126 (2014)
- Skordic, C., Zlosnik, T.: (2019). [arXiv:1905.09465](https://arxiv.org/abs/1905.09465)
- Zwicky, F.: *Helv. Phys. Acta* **6**, 110 (1933)